Palaeogeography, Palaeoclimatology, Palaeoecology 509 (2018) 24–32

Contents lists available at ScienceDirect

Palaeogeography, Palaeoclimatology, Palaeoecology

journal homepage: www.elsevier.com/locate/palaeo

Trend of increasing Holocene summer precipitation in arid central Asia: Evidence from an organic carbon isotopic record from the LJW10 loess section in Xinjiang, NW China

Haichao Xie[a,*], Huiwen Zhang[a,b], Jianying Ma[c], Guoqiang Li[a], Qiang Wang[a], Zhiguo Rao[a,d], Wei Huang[a], Xiaozhong Huang[a], FaHu Chen[a,e]

[a] MOE Key Laboratory of West China's Environmental System, College of Earth and Environmental Sciences, Lanzhou University, Lanzhou 730000, China
[b] State Key Laboratory Breeding Base of Desertification and Aeolian Sand Disaster Combating, Gansu Desert Control Research Institute, Lanzhou 730000, China
[c] Xinjiang Institute of Ecology and Geography, Chinese Academy of Sciences, Urumqi 830011, Xinjiang, China
[d] College of Resources and Environmental Sciences, Hunan Normal University, Changsha 410081, China
[e] Chinese Academy of Sciences Center for Excellence in Tibetan Plateau Earth Sciences, Beijing 100101, China

ARTICLE INFO

Keywords:
Climate change
Wettest late Holocene
$\delta^{13}C_{org}$
Westerlies
NAO/AO
Circumglobal teleconnection

ABSTRACT

Due to the lack of reliable climatic proxies, the variability of precipitation in "Westerlies-dominated" arid central Asia (ACA) during the Holocene is debated. Here, we present a high-resolution (ca. 100 years per sample) organic carbon isotopic composition ($\delta^{13}C_{org}$) record from bulk samples from the Lujiaowan10 section in the northern piedmont of the Tienshan Mountains, Xinjiang Province, northwestern China. A robust chronology is provided by K-feldspar pIRIR dating. During the early to middle Holocene, from 12 ka to 6 ka (1 ka = 1000 years ago), the $\delta^{13}C_{org}$ values are relatively invariant with an average of around −22.5‰. After about 6 ka, the $\delta^{13}C_{org}$ values exhibit an overall negative trend with the most negative value of −25.2‰ occurring in the uppermost part of the section, within the interval of Holocene soil formation. Our investigation of the relationship between modern climatic variables and surface soil $\delta^{13}C_{org}$ values from the region reveals a significant negative correlation between surface soil $\delta^{13}C_{org}$ and summer precipitation amount (June to August). Therefore, we used the calibration model between summer precipitation amount and surface soil $\delta^{13}C_{org}$ to quantitatively reconstruct the Holocene summer precipitation history of the study area. Our results indicate that summer precipitation in the region was the lowest (ca. 85 mm) during the early to middle Holocene (12–6 ka); however, after 6 ka, the precipitation increased continuously to about 137 mm per year at the present. Our reconstruction is generally consistent with climate simulation results and with regional effective moisture records. Thus, we conclude that the highest summer precipitation, and therefore the wettest climate, occurred in the late Holocene. Decreasing Northern Hemisphere summer insolation may have effected a change in the CGT (circumglobal teleconnection) from a positive to negative phase and, together with more negative trends in AO (Arctic Oscillation) or NAO (North Atlantic Oscillation), may have been responsible for the observed pattern of summer precipitation evolution.

1. Introduction

Westerlies or Prevailing Westerlies is used to mark westerly surface winds that flow in an approximately constant direction within the Ferrel circulation cells (Palmén and Newton, 1969). These winds are generally recognized above the ocean, while above the continent they are very deformed and lose their "prevailing" characteristics. On the other hand, it is Polar Front (Palmén and Newton, 1948), instead of Westerlies that considered as the main creator of weather and climate in middle latitudes (Bjerknes and Solberg, 1922), for example in Siberia (Hrnjak et al., 2014; Gavrilov et al., 2017), but except in areas of strong monsoon influence, such as in Asia. The mid-latitudes of the Asian continent can be divided into two distinct climatic regions: the monsoon dominated humid eastern-southern region, and the Westerly-dominated arid western region (Chen et al., 2008). Westerly-dominated Asia also called the arid central Asia (ACA) (Huang et al., 2015a), which is one of the most non-zonal arid regions in the world (Chen et al., 2008, 2010), where the scarcity of water and the fragility of the ecosystems render the region highly sensitive to variations in rainfall or effective moisture (Soucek, 2000; Seddon et al., 2016). Instrumental

* Corresponding author.
E-mail address: xiehch09@lzu.edu.cn (H. Xie).

https://doi.org/10.1016/j.palaeo.2018.04.006
Received 13 November 2016; Received in revised form 12 April 2018; Accepted 13 April 2018
Available online 20 April 2018
0031-0182/

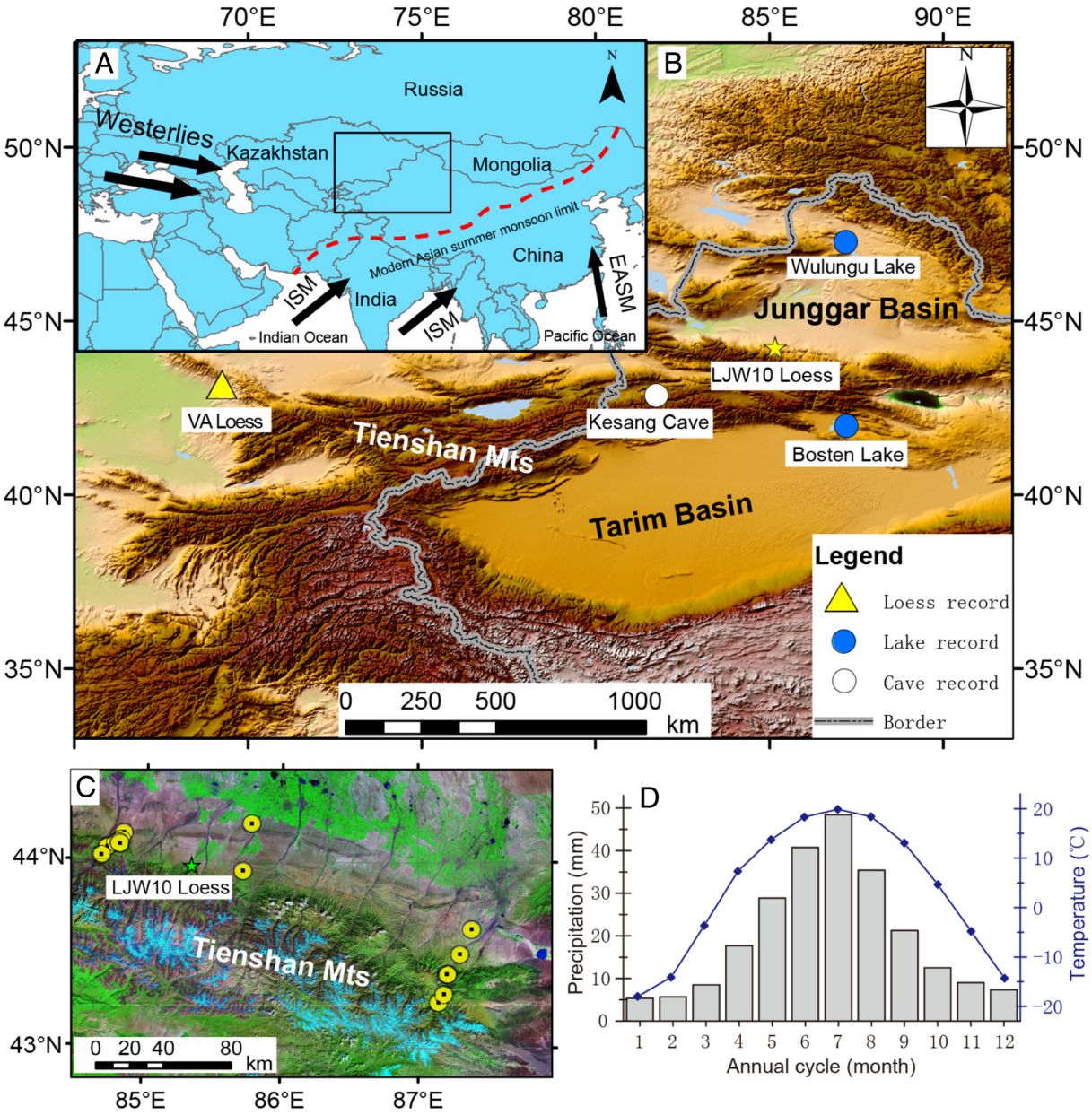

Fig. 1. (A) Location of the study area in Asia (rectangle), and the related climatic circulation systems that include the Westerlies, Indian summer monsoon (ISM) and East Asia summer monsoon (EASM) are also shown; (B) Geographical context of the LJW10 loess section (yellow star) in the northern fluvial plain of the Tienshan Mountains, northwest China. Other Holocene records used for comparison are also shown; (C) Locations of the surface soil samples taken along the northern slopes of the Tienshan Mountains. Details of the surface sample sites are given in Table 1; (D) Mean monthly temperature and precipitation at the LJW10 loess section (average of 1980–2010). (For interpretation of the references to colour in this figure legend, the reader is referred to the web version of this article.)

data demonstrate that, against the background of ongoing global warming, the climate of the region is becoming progressively wetter, in significant contrast to that of the Asian monsoon-dominated regions in eastern China (Shi et al., 2007; Chen et al., 2011). The nature of moisture and hydrological changes in ACA during the Holocene has long been debated (Li, 1990; Winkler and Wang, 1993; Morrill et al., 2003; Chen et al., 2008, 2016; Huang et al., 2009; Li et al., 2011; An et al., 2012; Cheng et al., 2012; Wang and Feng, 2013). Syntheses of relevant research concluded that the evolution of effective moisture in ACA was out-of-phase with that in the Asian monsoon-dominated regions during the Holocene (Chen et al., 2008), and even exhibited an anti-phased relationship on a multi-centennial time-scale over the past millennium (Chen et al., 2010). In addition, rather arid conditions are suggested for the early Holocene (12–8 ka), humid conditions in the mid-late Holocene, with the most humid interval from 8 ka to 6 ka (Chen et al., 2008). In contrast, however, the stalagmite oxygen isotopic ($\delta^{18}O$) records from Kesang Cave (42.8667°N, 81.7500°E, altitude ~2000 m above mean sea level (AMSL.)) (Fig. 1B) reveal a similar trend of variation of moisture/precipitation to that in monsoonal Asia (wet and warm during the early-middle Holocene) (Cheng et al., 2012); however, it has recently been determined that the stalagmite $\delta^{18}O$ records cannot be used as a summer monsoon proxy (Liu et al., 2015). This finding is supported by a pollen-based effective moisture record (*Artemisia/Chenopodiaceae* (A/C) ratio) from the Yili section (Fig. 1B), which also indicates that the wettest period occurred during the early Holocene (Li et al., 2011). Climatic reconstructions based on these types of proxy record, with a relatively wet climate in ACA in the early to middle Holocene, have long been interpreted as reflecting the penetration of the Asian summer monsoon into ACA (Winkler and Wang, 1993; Rhodes et al., 1996; Morrill et al., 2003; Li et al., 2011; Cheng

et al., 2012). Recent results from loess deposits indicate a persistent wetting trend in the core zone of the "Westerlies-dominated climatic regime" (Huang et al., 2015a) during the Holocene (Chen et al., 2016). Overall, various proxy climate records from lake sediments (e.g., Chen et al., 2008; Morrill et al., 2003; Huang et al., 2009; Wang and Feng, 2013; Jiang et al., 2013), peatlands (Hong et al., 2014), speleothems (Cheng et al., 2012) and loess deposits (Chen et al., 2016) present a somewhat complex picture of the evolution of moisture and precipitation in this region during the Holocene. As they are all climatically controlled by the Westerlies, which indicated that they should have shown the same precipitation or effective moisture evolution trend. Although they may have differences on height, vegetation cover and terrain, etc., which considered could only introduce differences in the amplitude of the fluctuations of these records. Discrepancies between the various records may partially result from differences in the climatic significance of the various proxies used, and therefore a reliable and unequivocal Holocene quantitative precipitation record is still needed for ACA.

Loess deposits are widely distributed on the northern slopes of the Tienshan and Kunlun Mountains, and in Yili Valley (Liu, 1985; Feng et al., 2011). Loess is regarded as an ideal paleoenvironmental archive because of its relatively simple source and continuous deposition (Forster and Heller, 1994; Bronger et al., 1998; Ye et al., 2003; Song and Shi, 2010; Yang et al., 2014), and has been widely used to reconstruct climatic variations on glacial-interglacial (Ding et al., 2002; Feng et al., 2011) and longer time-scales (Yang and Ding, 2006). However, the use of magnetic parameters such as the magnetic susceptibility, which have been successfully applied to the loess-paleosol sequences of the Chinese Loess Plateau (Zhou et al., 1990; Kukla et al., 1988) are much less effective climatic proxies for the Xinjiang loess because of the complexity of the magnetic enhancement mechanism (Song et al., 2010; Jia et al., 2012, 2013). Although the environmental magnetic proxies of χ_{fd} and χ_{ARM}/SIRM have been used to reconstruct variations in pedogenic intensity, and therefore in effective moisture, in Xinjiang (Jia et al., 2012, 2013; Xia et al., 2014; Chen et al., 2016), they cannot at present be used to provide quantitative records of precipitation or effective moisture.

Terrestrial plants mainly use the C_3 and C_4 photosynthetic pathways. The carbon isotopic composition ($\delta^{13}C$) of modern C_3 plants ranges from −20.0‰ to −34.0‰, with the most common value around −27.0‰ (Deines, 1980; O'Leary, 1981, 1988; Farquhar et al., 1989). The relationship between the $\delta^{13}C$ of modern C_3 plants and climatic factors has been explored for decades, with most of the findings indicating that the $\delta^{13}C$ values of modern C_3 plants are negatively correlated with precipitation (Liu et al., 2005a; Wang et al., 2003; Zheng and Shangguan, 2007; Kohn, 2010; Ma et al., 2012; Rao et al., 2017). The change in $\delta^{13}C_{org}$ during the processes of burial and decomposition of plant remains can be regarded as a "systematically positive excursion" of about ca. 1‰ (Melillo et al., 1989; Wang et al., 2008; Rao et al., 2013b). In addition, microbial activity has been demonstrated not to significantly affect the $\delta^{13}C_{org}$ values of loess, based on a comparison of the $\delta^{13}C$ of long chain n-alkanes and loess $\delta^{13}C_{org}$ values in the Chinese Loess Plateau (Liu et al., 2005b). Therefore, the values of $\delta^{13}C_{org}$ ($\delta^{13}C$ of organic matter from bulk loess deposits and surface soil) can be regarded as an effective precipitation proxy (Hatté et al., 2001; Chen et al., 2006; Rao et al., 2012, 2017). $\delta^{13}C_{org}$ has been widely used for the reconstruction of precipitation in European loess (Hatté and Guiot, 2005), as well as growing season precipitation (Lee et al., 2005; Rao et al., 2013a) and annual precipitation (Feng et al., 2008), in the Chinese Loess Plateau. Based on the results of investigations of modern plants (Ma et al., 2007a, 2007b), as well as $\delta^{13}C_{org}$ records from loess-paleosol sequences in ACA (e.g., from the AXK loess section in Xinjiang Province, NW China (Fig. 1B; Rao et al., 2013a) and the VA section in Kazakhstan (Fig. 1B; Ran and Feng, 2014)), we can conclude that vegetation in ACA was dominated by C_3 species since at least the last glacial. Thus, $\delta^{13}C_{org}$ in this region can potentially be used as a paleoprecipitation proxy, or even as a means of quantitatively reconstructing precipitation.

In the present study, we report the results of $\delta^{13}C_{org}$ measurements of bulk samples from a Holocene loess-paleosol section (LJW10) with a relatively high organic matter content, located on the northern piedmont of the Tienshan Mountains (Chen et al., 2016). The chronology of the section is well-constrained by K-feldspar pIRIR luminescence dating (Li et al., 2015). In addition, the $\delta^{13}C_{org}$ values of surface soils from the Tienshan area (Zhang, 2010) were investigated to determine their relationship with summer precipitation. Based on this relationship, we used the $\delta^{13}C_{org}$ record from the LJW10 section to quantitatively reconstruct the history of regional summer precipitation during the Holocene.

2. Study area, materials and methods

2.1. The study section

The LJW10 loess section (43.9747°N, 85.3361°E; altitude 1462 m AMSL.) is located on the northern piedmont of the Tienshan Mountains in Xinjiang Province, in arid NW China (Fig. 1B). The climate of the region is controlled by the Westerlies circulation (Fig. 1A; Huang et al., 2015a). Mean annual temperature ranges from ca. 1.53 °C to 4.58 °C, and precipitation occurs mainly during the summer season (June to August) (ca. 52% of annual precipitation, Fig. 1D), with mean annual precipitation from ca. 168 mm to 341 mm (1981 to 2010); thus, the region has a typical temperate continental climate (all meteorological data are from a newly developed high spatial resolution LZU0025 database) (Wu et al., 2014). The current vegetation is mainly temperate steppe, consisting for example of the C_3 plants *Seriphidium gracilescens* and *C. turkestanic*. C_4 plants such as *Atriplex tatarica* Linn. occur in the region but are absent from the study site.

Based on the previously-determined K-feldspar pIRIR chronology, the uppermost 2.8 m of the LJW10 section were deposited during the past 15.88 kyr (1 kyr = 1000 years) (Li et al., 2015). We selected the uppermost 2.3 m of the section, which was mainly deposited during the Holocene, for $\delta^{13}C_{org}$ analyses. This part of the section can be divided into two main units: the uppermost 1.7 m paleosol layer (Unit 1) and the lower 0.6 m eolian loess layer (Unit 2) (Fig. 2A). Unit 1 consists of three yellowish-brown weakly-developed pedogenic sub-layers, with two intercalated relatively well-developed paleosol sub-layers (Fig. 2A, F). Modern plant roots were only observed in the uppermost 20 cm of Unit 1. Unit 2 consists mainly of a massive yellowish loess layer, with very scarce biochannels or other traces of biological activity. The age-depth model of the section, based on K-feldspar pIRIR dating, is shown in Fig. 2B and has been reported previously (Li et al., 2015), as was the environmental magnetic record (Fig. 2C; Chen et al., 2016).

2.2. TOC and $\delta^{13}C_{org}$ measurements

A total of 115 bulk samples at a 2-cm interval were collected from the section in 2010. All samples were used for $\delta^{13}C_{org}$ measurements, and 57 of them for TOC (total organic carbon) measurements. The samples were air-dried at room temperature, ground and passed through a 74 μm mesh after removing any visible modern roots. Then, 1.0–1.5 g of sample were digested for 6 h with < 10% hydrochloric acid (HCl) at room temperature and then heated in a water bath for about 2 h at 80 °C to completely remove carbonate. The samples were then washed several times with deionized water in a permeable crucible until the suspension was neutral (pH > 6). Finally, the samples were oven-dried at 80 °C and then ground again.

A total of 57 pretreated samples were used for measurements of TOC content using an HT 1300 Total Carbon Analyzer (Analytik Jena AG instrument). All 115 pretreated samples were weighed, and then sealed in Sn boats for $\delta^{13}C_{org}$ measurements using a stable isotope ratio mass spectrometer (Thermo Fisher Scientific (Bremen) HmbH, Delta

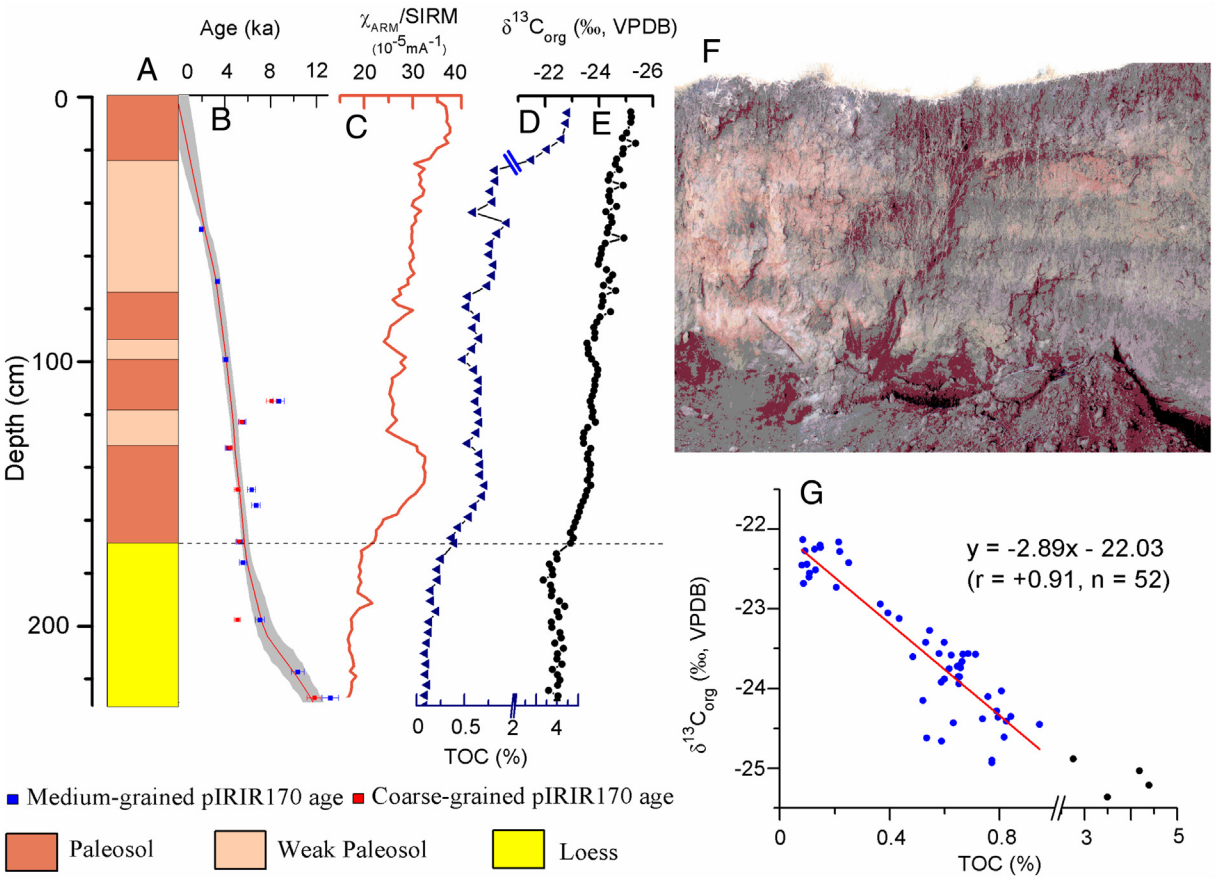

Fig. 2. (A) Lithology; (B) Age-depth model (after Li et al., 2015); (C) Ratio of anhysteretic to saturation isothermal remanence (χ_{ARM}/SIRM), an environmental magnetic proxy for pedogenic intensity (after Chen et al., 2016); (D) Total organic carbon content (TOC); (E) $\delta^{13}C_{org}$ versus depth in the LJW10 loess section. (F) Photo of the LJW10 section; (G) The correlation between TOC and $\delta^{13}C_{org}$ is shown in the bottom right-hand corner, p(a) < 0.01.

Plus). The results of measurements of four different international standards that include Glucine ($\delta^{13}C = -33.30‰$, VPDB), Puge ($\delta^{13}C = -12.60‰$, VPDB), Collagen ($\delta^{13}C = -9.00‰$, VPDB) and Soil ($\delta^{13}C = -27.46‰$, VPDB), all of which indicated that the standard deviation of the instrumental measurements was < 0.15‰. All the $\delta^{13}C_{org}$ data reported in this study are expressed as per mil (‰) relative to the Vienna Pee Dee belemnite (VPDB). The $\delta^{13}C_{org}$ results were calculated as follows:

$$\delta^{13}C_{org} = (R_{sample}/R_{standard} - 1) \times 1000. \quad (1)$$

Here R_{sample} and $R_{standard}$ are the $^{13}C/^{12}C$ ratios of the samples and the VPDB standard, respectively. Sample pretreatment and measurements were conducted at the Key Laboratory of Western China's Environmental Systems (Ministry of Education), Lanzhou University.

2.3. Results from surface soil samples

The expression for the description of carbon isotopic fractionation in the leaves of modern C_3 plants can be expressed as:

$$\Delta = a + (b - a) \times (p_i/p_a). \quad (2)$$

Here Δ is the fractionation value of C_3 plants in the process of CO_2 uptake and fixation, a is the carbon isotopic fractionation in leaf surface cells during CO_2 diffusion (ca. 4.4‰), b is the net fractionation caused by carboxylation (ca. 29‰), and p_a and p_i are the ambient and intercellular partial pressures of CO_2 in mesophyll cells (Farquhar et al., 1989). An increase in precipitation, or in effective moisture, can increase the stomatal conductance, thereby reducing p_i and Δ and resulting in a negative carbon isotopic composition ($\delta^{13}C$) of C_3 plants (Farquhar et al., 1989).

In this study, we have also selected 15 modern surface soil samples collected from the northern slopes of the Tienshan Mountains along an annual precipitation gradient of ca. 201 mm to 270 mm (average values from 1981 to 2010); the data have been reported previously (Fig. 1C, Table 1; Zhang, 2010). We used three criteria for selecting these samples. Firstly, the altitude should be < 2240 m, because we found that at altitudes > 2240 m the vegetation changed from grassland to coniferous forest, and the accompanying changes in temperature would be expected to strongly influence the $\delta^{13}C_{org}$ values. On the other hand, at altitudes < 2240 m, precipitation would be expected to be the predominant factor determining $\delta^{13}C_{org}$ (Zhang, 2010). Secondly, the local plants at the surface soil sampling site should be dominated by C_3 plants, as was the case at the site of the LJW10 section. Thirdly, the $\delta^{13}C_{org}$ values of plants should be more negative than the local surface soil, because the effect of the decomposition of plant remains would be expected to enrich the soil $\delta^{13}C_{org}$ in $\delta^{13}C$ during the interval of burial (Melillo et al., 1989; Wang et al., 2008). The modern climatic characteristics of the selected sampling sites were obtained from a LZU0025 grid climate dataset with a spatial resolution of 0.025° × 0.025° (2.8 × 2.8 km) over China (Wu et al., 2014). Information about the selected surface soil sample sites (Fig. 1D) and relevant climatic and $\delta^{13}C$ data are listed in Table 1.

3. Results

3.1. Variation of TOC and $\delta^{13}C_{org}$ within the LJW10 loess section

The age-depth curve for the LJW10 loess section (from Li et al.,

Table 1
The modern surface soil samples used for $\delta^{13}C_{org}$ analyses: site locations, climatic characteristics, and average values from 1981 to 2010.

Sites	Altitude (m AMSL.)	Longitude (°)	Latitude (°)	In situ plant names	Photosynthetic types	Annual precipitation (mm)	Summer precipitation (mm)	Mean annual temperature (°C)	$\delta^{13}C_{org}$ (‰)
SW	617	85.7736	44.2061	*Seriphidium gracilescens*	C3	201	72	6.7	−22.4
SHZ	1142	85.7144	43.9525	*Poa tianschanica* (Regel) Hack. ex O. Fedtsch	C3	227	105	6.2	−24.7
KZK	1320	87.3903	43.6414	*Peganum harmala* L	C3	235	106	8.1	−23.0
MLG	1385	84.7164	44.0700	*Seriphidium gracilescens*	C3	245	131	7.0	−25.7
DSZ	1392	84.8347	44.1450	*Stipa capillata*	C3	235	119	7.0	−24.6
MLG	1420	84.6725	44.0256	*Festuca ovina*	C3	256	142	6.9	−24.8
KZK	1610	87.3042	43.5078	*Leymus tianschanicus*	C3	239	124	7.1	−24.9
MLG	1617	84.7761	44.0886	*Seriphidium gracilescens*	C3	270	152	6.7	−25.5
DSZ	1645	84.8172	44.1108	*Seriphidium gracilescens*	C3	254	138	6.4	−24.5
NTZ-HX	1757	87.215	43.4003	*Phlomis oreophila* Kar. et Kir	C3	247	139	6.5	−25.0
NTZ	1760	87.2097	43.3986	*Leymus tianschanicus*	C3	244	135	6.6	−25.4
DSZ	1785	84.8000	44.0953	*Phlomis oreophila* Kar. et Kir	C3	267	150	6.3	−26.7
BYG	1850	84.8061	44.0850	*Leymus tianschanicus*	C3	274	156	6.0	−25.8
NTZ-HX	2045	87.1472	43.2472	*C. turkestanic*	C3	257	156	6.6	−25.5
NTZ-HX	2075	87.1881	43.2925	*Agropyron cristatum* (Linn.) Gaertn	C3	254	151	6.7	−24.9

SW-Shawan County, SHZ-Shihezi City, KZK-Kazikou, MLG-Maoliugou, DSZ-Dushanzi, NTZ-HX-Nantaizi-Houxia, NTZ – Nantaizi, BYG-Bayingou (after Zhang, 2010).

2015), the variation of TOC content and $\delta^{13}C_{org}$ with depth, and the χ_{ARM}/SIRM record (from Chen et al., 2016), are illustrated in Fig. 2. The χ_{ARM}/SIRM record reflects variations in the content of fine ferrimagnetic grains produced during weathering and pedogenesis. In Unit 2 (below 1.7 m, loess of early to middle Holocene age) the $\delta^{13}C_{org}$ values are relatively positive and fluctuate between −23.3‰ and −21.9‰ with an average of −22.5‰ (Fig. 2E). The $\delta^{13}C_{org}$ values shift abruptly to more negative values above 1.7 m depth (Unit 1, paleosol) and maintain a decreasing trend towards the top of the section, which has the most negative value of −25.2‰. The three relatively strongly-developed pedogenic sub-layers exhibit slightly negative $\delta^{13}C_{org}$ values, while the interbedded relatively weakly-developed pedogenic sub-layers exhibit slightly positive $\delta^{13}C_{org}$ values (Fig. 2E). Given that during the process of organic matter decomposition, the $\delta^{13}C_{org}$ values will become more positive normally by 2–3‰ (Melillo et al., 1989; Connin et al., 2001; Wang et al., 2008), the overall negative $\delta^{13}C_{org}$ values from the section indicate that the vegetation was almost entirely dominated by C_3 plants during the Holocene. It has also been reported that since the last glacial the vegetation in the Yili Valley in the western Tienshan mountain region was dominated by C_3 plants (Rao et al., 2013b).

The changes in TOC concentration within the section follow the same trend as the $\delta^{13}C_{org}$ values, with the minimum value of 0.08% at the bottom of the section and the maximum value of 0.82% at the top. The record for the uppermost 26 cm, which is clearly influenced by modern plant root penetration, has TOC concentrations between 2.28% and 4.48% (Fig. 2D). The application of linear regression analysis (after removing the samples from the uppermost 26 cm) to the TOC and $\delta^{13}C_{org}$ records produced a significant negative correlation with a coefficient of determination of 0.82 (Fig. 2G). This indicates that the enhanced C_3 plant density may have been mainly responsible for the trend of increasing TOC since about 6 ka.

3.2. Modern relationship between $\delta^{13}C_{org}$ and climate

The relationship between the $\delta^{13}C_{org}$ values of modern surface soils and climatic factors has been widely investigated in the Chinese Loess Plateau (Liu et al., 2005c), northern China (Lee et al., 2005; Feng et al., 2008) and Europe (Hatté and Guiot, 2005). Unfortunately, little comprehensive research has been conducted in ACA, especially in the Tienshan Mountains area, where loess deposits are widespread (Song and Shi, 2010). Some studies have suggested that $\delta^{13}C_{org}$ is a temperature proxy (Wang et al., 2013a). While, it can be demonstrated that the temperature variations could only affect the $\delta^{13}C_{org}$ values of surface soil via changing the relative abundance of C_3 and C_4 plants (Zhang et al., 2003b). Thus, in areas dominated by C_3 plants, such as ACA, the temperature effect on C_3 plants can be neglected. Most researchers have obtained a very significant negative correlation between the $\delta^{13}C_{org}$ of surface soil and annual precipitation (Zhang et al., 2003a; Feng et al., 2008; Diefendorf et al., 2010), or summer precipitation (Lee et al., 2005). However, in most cases the correlation functions between $\delta^{13}C_{org}$ of surface soil and precipitation are different in different regions (Lee et al., 2005; Hatté and Guiot, 2005), which means that it is necessary to determine specific correlation functions for individual regions to reconstruct paleoprecipitation variation.

Here, we analyzed the correlation among $\delta^{13}C_{org}$ of these 15 selected surface soil samples from Tienshan Mountain areas and their corresponding climatic factors that including annual precipitation, growing season precipitation (May to September) and summer precipitation (June to August). Results show that both the summer precipitation and growing season precipitation have obviously linear correlation with surface soil $\delta^{13}C_{org}$ (summer precipitation, $r = +0.82$, $p(a) < 0.01$, $n = 15$; growing season precipitation, $r = +0.83$, $p(a) < 0.01$, $n = 15$). While annual precipitation and surface soil $\delta^{13}C_{org}$ are poorly correlated (Fig. 3A). Therefore, we can conclude that $\delta^{13}C_{org}$ can be used to quantitively reconstruct summer precipitation or growing season precipitation in the Tienshan Mountain areas. The linear regression function between $\delta^{13}C_{org}$ and summer precipitation can be expressed as:

$$\text{Summer precipitation} = -18.14 \times \delta^{13}C_{org} - 319.72 \ (r = +0.82, p(a) < 0.01, n = 15) \quad (3)$$

This relationship is used to reconstruct Holocene summer precipitation with a 95% degree of confidence (Fig. 3A). It should be noted that 1‰ of the $\delta^{13}C_{org}$ values have been corrected to exclude the effect of decomposition, which usually occurs during the burial stage after the

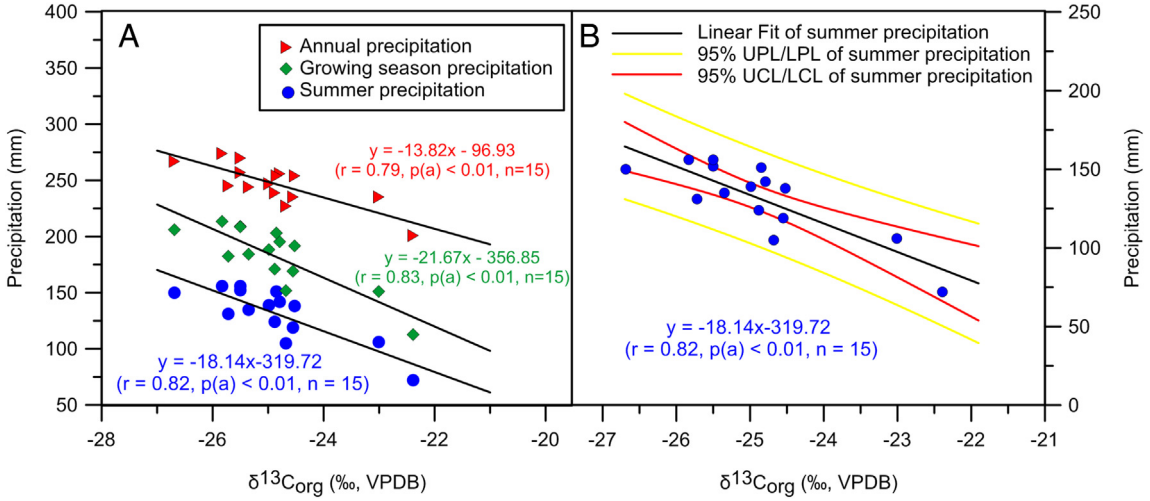

Fig. 3. (A) Scatter plots showing the linear relationship between annual precipitation (red filled triangles), growing season precipitation (May to September) (green filled diamonds) and summer precipitation (June to August) (blue filled circles) with surface soil $\delta^{13}C_{org}$; (B) Linear fit between summer precipitation (June to August) (blue filled circles) and surface soil $\delta^{13}C_{org}$, with the 95% UPL and LPL (Upper and Lower Prediction Limit) bands (yellow line) and the 95% UCL and LCL (Upper and Lower Confidence Limit) bands (red line). (For interpretation of the references to colour in this figure legend, the reader is referred to the web version of this article.)

death of the plants (Fig. 4A; Wang et al., 2008).

4. Discussion

The $\delta^{13}C_{org}$ record of the LJW10 loess section indicates that the local vegetation was almost entirely dominated by C_3 plants during the Holocene. $\delta^{13}C_{org}$ records from other two loess sections in arid central Asia, the AXK loess section in Yili Valley in arid northwest China (Fig. 1B; Rao et al., 2013b), and the VA loess section in Kazakhstan (Fig. 4C; Ran and Feng, 2014), also show that these regions were dominated by C_3 plants during the Holocene. In the Yili loess section, the $\delta^{13}C_{org}$ values ranged from −20‰ to −26‰ during the Holocene, while in the VA section they ranged from −22.5‰ to −25‰. These values are all within the expected range of C_3 plants, given a 2–3‰ positive shift during the process of organic matter decomposition during soil formation (Melillo et al., 1989; Wang et al., 2008; Rao et al., 2013b). Consequently, we conclude that during the Holocene, arid central Asia was dominated by C_3 plants, at least in the loess-covered areas.

In the AXK loess section in Yili Valley, northwest China (Fig. 1B), the $\delta^{13}C_{org}$ record exhibits a general negative trend during the interval of Holocene paleosol formation, although there is no accurate chronology (Rao et al., 2013b). In the VA section, Kazakhstan (Fig. 1B), the $\delta^{13}C_{org}$ values fluctuated from 12 to 5 ka, and then abruptly commenced a negative trend after 5 ka (Fig. 4C; Ran and Feng, 2014). Therefore, it seems that the persistent negative trend of $\delta^{13}C_{org}$ values since the mid-Holocene (~6 ka), documented in the LJW10 loess section (Fig. 2E), is a common phenomenon in the core area of "Westerlies-dominated" ACA. This implies that precipitation has been increasing in the region since the mid-Holocene.

Our reconstructed modern summer precipitation was 155 mm, with a 95% confidence coefficient UCL (Upper Confidence Limit) of 167 mm and LCL (Lower Confidence Limit) of 142 mm (Fig. 4A). Although this estimate is slightly higher than the value of 125 mm obtained for the past 30 years (1980–2010), it is within the range of summer precipitation fluctuations (85–203 mm) over the past 30 years (1981–2010), which demonstrates that our reconstruction is reliable. The reconstructed summer precipitation record for the LJW10 section (Fig. 4A) indicates that during the early to middle Holocene (12–6 ka) mean summer precipitation varied around 85 mm with few apparent changes, and then generally increased from ~6 ka until the present. Thus, our results demonstrate an increasing trend of summer precipitation from the middle to late Holocene (commencing at ~6 ka). The reality of this trend is supported by the trend of increasing pedogenic intensity during the same interval indicated by an environmental magnetic proxy (Fig. 4B; Chen et al., 2016).

The evolution of moisture in the core area of "Westerlies-dominated" ACA during the Holocene (Huang et al., 2015a) has been studied for decades (Chen et al., 2008, 2016; Li et al., 2011; Cheng et al., 2012; Wang et al., 2013b; Hong et al., 2014). However, there has been no consensus regarding the significance of the results, partly because of uncertainties in the interpretation of many of the proxies used, and because of the lack of quantitative precipitation reconstructions. In the case of the LJW10 loess section, the climatic significance of the $\delta^{13}C_{org}$ record is relatively unambiguous, and in addition the record has a robust chronology provided by K-feldspar pIRIR dating (Li et al., 2015). Moreover, the study section is located within the core zone of "Westerlies-dominated" ACA (Huang et al., 2015a) and in addition our quantitative summer precipitation record is supported by previous moisture reconstructions for the study area (Fig. 1B, 4C-H). The record from Wulungu Lake in northern Xinjiang reveals a trend of increasing lake level since the early Holocene (Fig. 4D; Liu et al., 2008), indicating increasing wetness. In a pollen record from Bosten Lake in southern Xinjiang there is a trend of decreasing representation of the drought-tolerant desert plant *Ephedra* since 8 ka, indicating a trend of increasing wetness (Fig. 4E; Huang et al., 2009). An integrated moisture record from northern Xinjiang, based mainly on lake archives, also exhibits a generally increasing trend since 12 ka (Fig. 4F; Wang and Feng, 2013). In summary, all the available evidence indicates that, in the core area of the "Westerlies-dominated" ACA, the early Holocene was relatively dry compared to the middle and late Holocene (An et al., 2012; Leroy et al., 2013, 2014; Long et al., 2014; Chen et al., 2016).

Climate modelling results from the TraCE-21 dataset that consider both external and internal forcing (changes in insolation, atmospheric greenhouse gases, meltwater fluxes and continental ice sheets) indicate that both summer and winter precipitation in the core area of ACA increased since 12 ka (Liu et al., 2009, 2014). Recent transient simulation results conducted using the Kiel Climate Model (KCM), a coupled atmosphere-ocean-sea ice general circulation model, indicate a wetting trend in ACA during the Holocene, especially an abrupt increase in summer precipitation in the middle Holocene (Fig. 4G; Zhang et al., 2017). Thus, our findings are highly consistent with those of climate

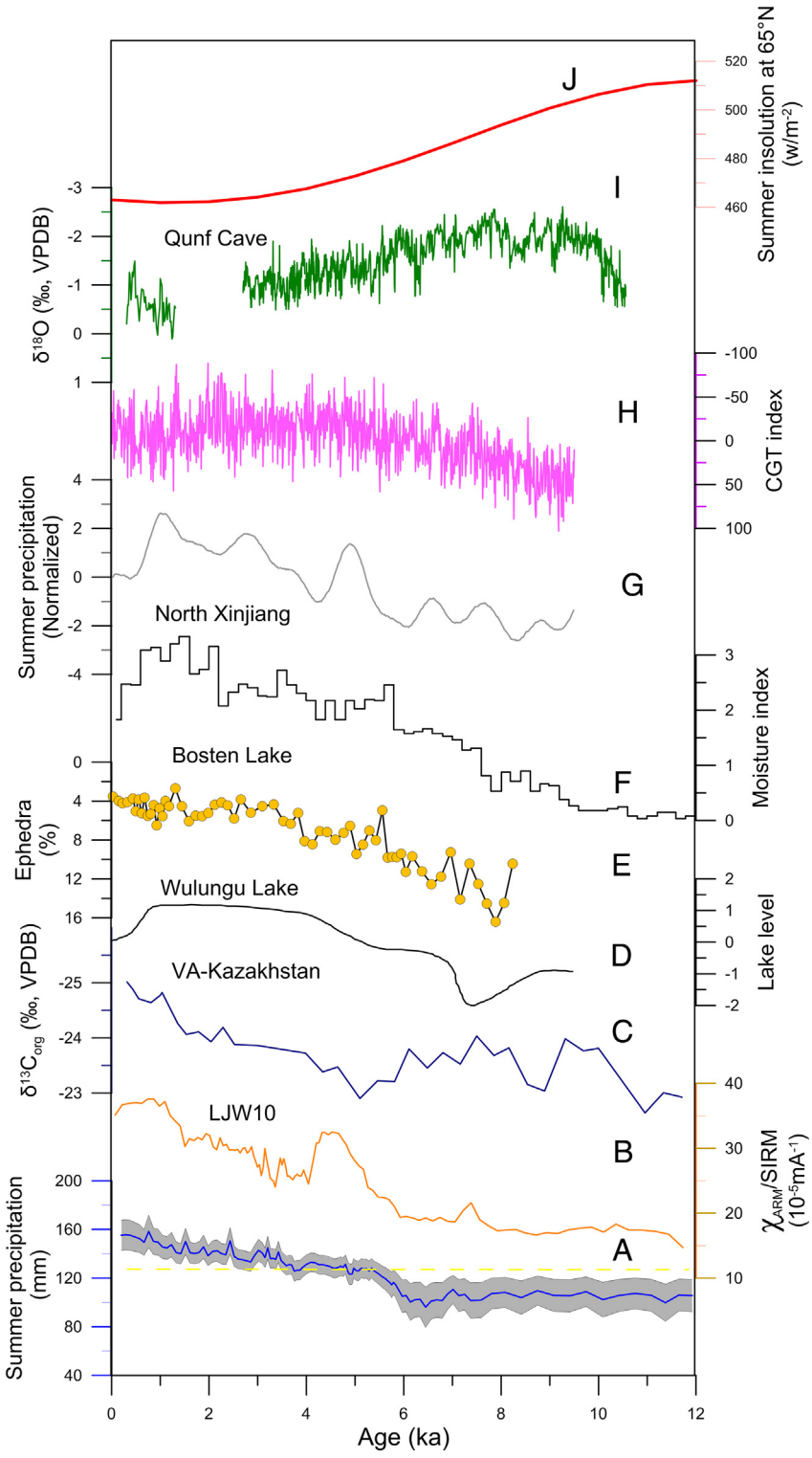

Fig. 4. Comparison of various Holocene proxy climate records from Asia. (A) Reconstructed summer precipitation from the LJW10 loess section during the Holocene. The grey band indicates the error of the 95% degree of confidence and the yellow dotted line is the mean modern summer precipitation (1981–2010); (B) χ_{ARM}/SIRM, a magnetic proxy for pedogenic intensity (Chen et al., 2016); (C) $\delta^{13}C_{org}$ record from the VA loess section, Kazakhstan (Ran and Feng, 2014); (D) Lake level of Wulungu Lake (Liu et al., 2008); (E) *Ephedra* percentages from a sediment core from Bosten Lake (Huang et al., 2009); (F) Integrated moisture index from north Xinjiang (Wang and Feng, 2013); (G) Simulated summer precipitation of the ACA core area (Zhang et al., 2017); (H) Circumglobal teleconnection (CGT) index based on climate modelling results (Zhang and Jin, 2016). Negative values indicate negative phases of the CGT; (I) $\delta^{18}O$ record from Qunf Cave (Fleitmann et al., 2007); (J) Northern Hemisphere summer insolation (NHSI) (after Berger and Loutre, 1991). (For interpretation of the references to colour in this figure legend, the reader is referred to the web version of this article.)

modelling.

Previously published work has suggested that the pattern of Holocene moisture evolution in ACA was mainly caused by changing Westerly wind speed and evaporation upstream from the Mediterranean, Black, and Caspian Seas (Jin et al., 2012; Marković et al., 2014), and partly by changing evaporation rates resulting from variations in sea surface temperatures in the Northern Atlantic associated with freshwater input from the melting of the Laurentide ice sheet during the last deglaciation (Chen et al., 2008). A more negative trend of AO or NAO may also have contributed to the trend of increasing precipitation in the core area of ACA (Chen et al., 2016). Recent studies indicate that Holocene climatic variations, especially the evolution of precipitation in ACA, may have been caused by a recurrent circumglobal teleconnection (CGT) in the Northern Hemisphere summer mid-latitude circulation pattern (Ding and Wang, 2005). In response to decreasing Northern Hemisphere summer insolation (Fig. 4J; Berger and Loutre, 1991), the Indian summer monsoon decreased in strength during the Holocene (Fig. 4I; Fleitmann et al.,

2007), and both factors may have triggered a change in CGT from a positive to a negative phase (Fig. 4H; Zhang and Jin, 2016). The negative CGT phase, which persisted from the middle Holocene onwards, may have caused increased evaporation from the Indian Ocean. The increased evaporation may have been transmitted northwards along the eastern and northern margins of the Qinghai-Tibetan Plateau, resulting in heavy rainfall in the core area of ACA (Zhang and Jin, 2016). This scenario has been confirmed by studies of the modern climate (Huang et al., 2015b).

5. Conclusions

We present the results of $\delta^{13}C_{org}$ analyses of (i) bulk samples from a Holocene loess section (LJW10) in the northern piedmont of Tienshan, Xinjiang, in arid northwest China; and (ii) surface soil samples from the Tienshan area. We found that the $\delta^{13}C_{org}$ values were heaviest, with only minor fluctuations, during the early to middle Holocene, and then decreased continuously after ~6 ka. The $\delta^{13}C_{org}$ record of the loess section is consistent with that of other loess sections in the area, indicating that the $\delta^{13}C_{org}$ record represents a regional signal of changes in $\delta^{13}C_{org}$ in the study area during the Holocene. The $\delta^{13}C_{org}$ values of the surface soil samples are significantly correlated with summer precipitation, indicating that $\delta^{13}C_{org}$ in the study area is a valid summer precipitation proxy. We then applied this relationship to the $\delta^{13}C_{org}$ data from section LJW10 to quantitatively reconstruct summer precipitation during the Holocene. The results indicate that summer precipitation was very low (ca. 85 mm) and relatively invariant during the early to middle Holocene (12–6 ka), and then increased consistently after ~6 ka with the highest summer precipitation (137 mm) occurring at the present. Our record of reconstructed summer precipitation is consistent with other proxy precipitation results from loess, lake sediments, and lake level records and with climate simulation results for the study area.

Based on previously reported climatic simulation results, we conclude that the reconstructed trend of summer precipitation evolution may have resulted from the effect of decreasing Northern Hemisphere summer insolation in causing a phase change in CGT from positive to negative. In addition, the more negative trends of AO or NAO may have contributed to the trend of increasing precipitation in the core area of ACA during the Holocene.

Acknowledgments

We thank Mrs. Hui Hua and Mrs. Pingyu Zhang for their help in the laboratory, and Dr. Jan Bloemendal for critical discussion, constructive suggestions and English improvement. This work was supported by NSFC (grant nos. 41130102 and 41372180), and the Fundamental Research Funds for the Central Universities (Grant No. lzujbky-2016-244).

References

An, C.B., Lu, Y.B., Zhao, J.J., Tao, S.C., Dong, W.M., Li, H., Jin, M., Wang, Z.L., 2012. A high-resolution record of Holocene environmental and climatic changes from Lake Balikun (Xinjiang, China): implications for Central Asia. The Holocene 22, 43–52.

Berger, A., Loutre, M.F., 1991. Insolation values for the climate of the last 10 million years. Quat. Sci. Rev. 10, 297–317.

Bjerknes, J., Solberg, H., 1922. Life cycle of cyclones and the polar front theory of atmospheric circulation. Geofys. Publ. 3, 1–18.

Bronger, A., Winter, R., Heinkele, T., 1998. Pleistocene climatic history of East and Central Asia based on paleopedological indicators in loess-paleosol sequences. Catena 34, 1–17.

Chen, F.H., Rao, Z.G., Zhang, J.W., Jin, M., Ma, J.Y., 2006. Variations of organic carbon isotopic composition and its environmental significance during the last glacial on western Chinese Loess Plateau. Chin. Sci. Bull. 51, 1593–1602.

Chen, F.H., Yu, Z.C., Yang, M.L., Ito, E., Wang, S.M., Madsen, D.B., Huang, X.Z., Zhao, Y., Sato, T., Birks, H.J.B., Boomer, I., Chen, J.H., An, C.B., Wünnemann, B., 2008. Holocene moisture evolution in arid Central Asia and its out-of-phase relationship with Asian monsoon history. Quat. Sci. Rev. 27, 351–364.

Chen, F.H., Chen, J.H., Holmes, J., Boomer, I., Austin, P., Gates, J.B., Wang, N.L., Brooks, S.J., Zhang, J.W., 2010. Moisture changes over the last millennium in arid Central Asia: a review, synthesis and comparison with monsoon region. Quat. Sci. Rev. 29, 1055–1068.

Chen, F.H., Huang, W., Jin, L.Y., Chen, J.H., Wang, J.S., 2011. Spatiotemporal precipitation variations in the arid Central Asia in the context of global warming. Sci. China Earth Sci. 54, 1812–1821.

Chen, F.H., Jia, J., Chen, J.H., Li, G.Q., Zhang, X.J., Xie, H.C., Xia, D.S., Huang, W., An, C.B., 2016. A persistent Holocene wetting trend in arid Central Asia, with wettest conditions in the late Holocene, revealed by multi-proxy analyses of loess-paleosol sequences in Xinjiang, China. Quat. Sci. Rev. 146, 134–146.

Cheng, H., Zhang, P.Z., Spötl, C., Edwards, R.L., Cai, Y.J., Zhang, D.Z., Sang, W.C., Tan, M., An, Z.S., 2012. The climatic cyclicity in semiarid-arid Central Asia over the past 500,000 years. Geophys. Res. Lett. 39, L01705. http://dx.doi.org/10.1029/2011GL050202.

Connin, S.L., Feng, X., Virginia, R.A., 2001. Isotopic discrimination during long-term decomposition in an arid land ecosystem. Soil Biol. Biochem. 33, 41–51.

Deines, P., 1980. The isotopic composition if reduced organic carbon. In: Fritz, P., Fontes, J.C. (Eds.), Handbook of Environmental Isotope Geochemistry, the Terrestrial Environment. Vol. 1. Elsevier, Dordrecht, pp. 339–345.

Ding, Q.H., Wang, B., 2005. Circumglobal teleconnection in the northern Hemisphere summer. J. Clim. 18, 3483–3505.

Ding, Z.L., Ranov, V., Yang, S.L., Finaev, A., Han, J.M., Wang, G.A., 2002. The loess record in southern Tajikistan and correlation with Chinese loess. Earth Planet. Sci. Lett. 200, 387–400.

Diefendorf, A.F., Mueller, K.E., Wing, S.L., Koch, P.L., Freeman, K.H., 2010. Global patterns in leaf $\delta^{13}C$ discrimination and implications for studies of past and future climate. Proc. Natl. Acad. Sci. U. S. A. 107, 5738–5743.

Farquhar, G.D., Ehleringer, J.R., Hubick, K.T., 1989. Carbon isotope discrimination and photosynthesis. Annu. Rev. Plant Physiol. 40, 503–537.

Feng, Z.D., Wang, L.X., Ji, Y.H., Guo, L.L., Lee, X.Q., Dworkin, S.I., 2008. Climatic dependency of soil organic carbon isotopic composition along the S-N transect from 34°N to 52°N in central-east Asia. Palaeogeogr. Palaeoclimatol. Palaeoecol. 257, 335–343.

Feng, Z.D., Ran, M., Yang, Q.L., Zhai, X.W., Wang, W., Zhang, X.S., Huang, C.Q., 2011. Stratigraphies and chronologies of late Quaternary loess-paleosol sequences in the core area of the central Asian arid zone. Quat. Int. 240, 156–166.

Fleitmann, D., Burns, S.J., Mangini, A., Mudelsee, M., Kramers, J., Villa, I., Neff, U., Al-Subbary, A.A., Buettner, A., Hippler, D., Matter, A., 2007. Holocene ITCZ and Indian monsoon dynamics recorded in stalagmites from Oman and Yemen (Socotra). Quat. Sci. Rev. 26, 170–188.

Forster, T., Heller, F., 1994. Loess deposits from the Tajik depression (Central Asia): magnetic properties and paleoclimate. Earth Planet. Sci. Lett. 128, 501–512.

Gavrilov, M.B., Marković, S.B., Schaetzl, R.J., Tošić, I., Zeeden, C., Obreht, I., Sipos, G., Ruman, A., Putniković, S., Emunds, K., Perić, Z., 2017. Prevailing surface winds in Northern Serbia in the recent and past time periods; modern-and past dust deposition. Aeolian Res. 31, 117–129.

Hatté, C., Guiot, J., 2005. Palaeoprecipitation reconstruction by inverse modelling using the isotopic signal of loess organic matter: application to the Nussloch loess sequence (Rhine Valley, Germany). Clim. Dyn. 25, 315–327.

Hatté, C., Antoine, P., Fontugne, M., Lang, A., Rousseau, D.D., Zöller, L., 2001. $\delta^{13}C$ of loess organic matter as a potential proxy for paleoprecipitation. Quat. Res. 55, 33–38.

Hong, B., Gasse, F., Uchida, M., Hong, Y.T., Leng, X.T., Shibata, Y., An, N., Zhu, Y.X., Wang, Y., 2014. Increasing summer rainfall in arid eastern Central Asia over the past 8500 years. Sci. Rep. 4, 5279. http://dx.doi.org/10.1038/srep05279.

Hrnjak, I., Lukić, T., Gavrilov, M.B., Marković, S.B., Unkašević, M., Tošić, I., 2014. Aridity in Vojvodina, Serbia. Theor. Appl. Climatol. 115, 323–332.

Huang, X.Z., Chen, F.H., Fan, Y.X., Yang, M.L., 2009. Dry late-glacial and early Holocene climate in arid Central Asia indicated by lithological and palynological evidence from Bosten Lake, China. Quat. Int. 194, 19–27.

Huang, W., Chen, J.H., Zhang, X.J., Feng, S., Chen, F.H., 2015a. Definition of the core zone of the "westerlies-dominated climatic regime", and its controlling factors during the instrumental period. Sci. China Earth Sci. 58, 676–684.

Huang, W., Feng, S., Chen, J.H., Chen, F.H., 2015b. Physical mechanisms of summer precipitation variations in the Tarim Basin in northwestern China. J. Clim. 28, 3579–3591.

Jin, L.Y., Chen, F.H., Morrill, C., Otto-Bliesner, B., Rosenbloom, N., 2012. Causes of early Holocene desertification in arid Central Asia. Clim. Dyn. 38, 1577–1591.

Jia, J., Xia, D.S., Wang, B., Wei, H.T., Liu, X.B., 2012. Magnetic investigation of Late Quaternary loess deposition, Ili area, China. Quat. Int. 250, 84–92.

Jia, J., Xia, D.S., Wang, B., Zhao, S., Li, G.H., Wei, H.T., 2013. The investigation of magnetic susceptibility variation mechanism of Tienshan Mountains modern loess: Pedogenic or wind intensity model? Quat. Int. 296, 141–148.

Jiang, Q.F., Ji, J.F., Shen, J., Matsumoto, R., Tong, G.B., Qian, P., Ren, X.M., Yan, D.Z., 2013. Holocene vegetational and climatic variation in westerly-dominated areas of Central Asia inferred from the Sayram Lake in northern Xinjiang, China. Sci. China Earth Sci. 56, 339–353.

Kohn, M.J., 2010. Carbon isotope compositions of terrestrial C_3 plants as indicators of paleoecology and paleoclimate. Proc. Natl. Acad. Sci. U. S. A. 107, 19691–19695.

Kukla, G., Heller, F., Liu, X.M., Xu, T.C., Liu, T.S., An, Z.S., 1988. Pleistocene climates in China dated by magnetic susceptibility. Geology 16, 811.

Lee, X.Q., Feng, Z.D., Guo, L.L., Wang, L.X., Jin, L.Y., Huang, Y.S., Chopping, M., Huang, D.K., Jiang, W., Jiang, Q., Cheng, H.G., 2005. Carbon isotope of bulk organic matter: a proxy for precipitation in the arid and semiarid Central East Asia. Glob. Biogeochem. Cycles 19, 2833–2845. http://dx.doi.org/10.1029/2004GB002303.

Leroy, S.A.G., Kakroodi, A.A., Kroonenberg, S., Lahijani, H.K., Alimohammadian, H., Nigarov, A., 2013. Holocene vegetation history and sea level changes in the se corner

of the Caspian Sea: relevance to SW Asia climate. Quat. Sci. Rev. 70, 28–47.
Leroy, S.A., López-Merino, L., Tudryn, A., Chalié, F., Gasse, F., 2014. Late Pleistocene and Holocene palaeoenvironments in and around the Middle Caspian basin as reconstructed from a deep-sea core. Quat. Sci. Rev. 101, 91–110.
Li, J.J., 1990. The patterns of environmental changes since late Pleistocene in northwestern China. J. Quat. Sci. 3, e204.
Li, X.Q., Zhao, K.L., Dodson, J., Zhou, X.Y., 2011. Moisture dynamics in central Asia for the last 15 kyr: new evidence from Yili Valley, Xinjiang, NW China. Quat. Sci. Rev. 30, 3457–3466.
Li, G.Q., Wen, L.J., Xia, D.S., Duan, Y.W., Rao, Z.G., Madsen, D.B., Wei, H.T., Li, F.L., Jia, J., Chen, F.H., 2015. Quartz OSL and K-feldspar pIRIR dating of a loess/paleosol sequence from arid Central Asia, Tianshan Mountains, NW China. Quat. Geochronol. 28, 40–53.
Liu, T.S., 1985. Loess and the Environment. China Ocean Press, Beijing.
Liu, W.G., Feng, X.H., Ning, Y.F., Zhang, Q.L., Cao, Y.L., An, Z.S., 2005a. $\delta^{13}C$ variation of C_3 and C_4 plants across an Asian monsoon rainfall gradient in arid northwestern China. Glob. Chang. Biol. 11, 1094–1100.
Liu, W.G., Huang, Y.S., An, Z.S., Clements, S.C., Li, L., Prell, W.L., Ning, Y.F., 2005b. Summer monsoon intensity controls C_4/C_3 plant abundance during the last 35 ka in the Chinese Loess Plateau: carbon isotope evidence from bulk organic matter and individual leaf waxes. Palaeogeogr. Palaeoclimatol. Palaeoecol. 220, 243–254.
Liu, W.G., Ning, Y.F., An, Z.S., Wu, Z.H., Lu, H.Y., Cao, Y.N., 2005c. Carbon isotopic composition of modern soil and paleosol as a response to vegetation change on the Chinese Loess Plateau. Sci. China Earth Sci. 48, 93–99.
Liu, X.Q., Herzschuh, U., Shen, J., Jiang, Q.F., Xiao, X.Y., 2008. Holocene environmental and climatic changes inferred from Wulungu Lake in northern Xinjiang, China. Quat. Res. 70, 412–425.
Liu, Z.Y., Otto-Bliesner, B., He, F., Brady, E., Clark, P., Lynch-Steiglitz, J., Carlson, A., Curry, W., Brook, E., Jacob, R., Erickson, D., Kutzbach, J., Cheng, J., 2009. Transient simulation of deglacial climate evolution with a new mechanism for Bølling-Allerød warming. Science 325, 310–314.
Liu, Z.Y., Wen, X.Y., Brady, E.C., Otto-Bliesner, B., Yu, G., Lu, H.Y., Cheng, H., Wang, Y.J., Zheng, W.P., Ding, Y.H., Edwards, R.L., Cheng, J., Liu, W., Yang, H., 2014. Chinese cave records and the East Asia summer monsoon. Quat. Sci. Rev. 83, 115–128.
Liu, J.B., Chen, J.H., Zhang, X.J., Li, Y., Rao, Z.G., Chen, F.H., 2015. Holocene East Asian summer monsoon records in northern China and their inconsistency with Chinese stalagmite $\delta^{18}O$ records. Earth Sci. Rev. 148, 194–208.
Long, H., Shen, J., Tsukamoto, S., Chen, J.H., Yang, L.H., Frechen, M., 2014. Dry early Holocene revealed by sand dune accumulation chronology in Bayanbulak Basin (Xinjiang, NW China). The Holocene 24, 614–626.
Ma, J.Y., Chen, F.H., Zhang, H.W., Xia, D.S., 2007a. Spatial distribution characteristics of stable carbon isotope compositions in desert plant *Reaumuria soongorica* (Pall.) Maxim. Front. Earth Sci. China 1, 150–156.
Ma, J.Y., Chen, F.H., Xia, D.S., Zhang, H.W., 2007b. Stable carbon isotope composition of desert plant and surface soil in the Tarim Basin. J. Glaciol. Geocryol. 29, 144–148 (In Chinese with English abstract).
Ma, J.Y., Sun, W., Liu, X.N., Chen, F.H., 2012. Variation in the stable carbon and nitrogen isotope composition of plants and soil along a precipitation gradient in northern China. PLoS One 7, 324–328.
Marković, S.B., Ruman, A., Gavrilov, M.B., Stevens, T., Zorn, M., Komac, B., Perko, D., 2014. Modelling of the Aral and Caspian seas drying out influence to climate and environmental changes. Acta Geogr. Slov. 54–1, 143–161.
Melillo, J.M., Aber, J.D., Linkins, A.E., 1989. Carbon and nitrogen dynamics along the decay continuum: plant litter to soil organic matter. Plant Soil 115, 189–198.
Morrill, C., Overpeck, J.T., Cole, J.E., 2003. A synthesis of abrupt changes in the Asian summer monsoon since the last deglaciation. The Holocene 13, 465–476.
O'Leary, M.H., 1981. Carbon isotope fractionation in plants. Phytochemistry 20, 553–567.
O'Leary, M.H., 1988. Carbon isotopes in photosynthesis. Bioscience 38, 328–336.
Palmén, E., Newton, C.W., 1948. A study of the mean wind and temperature distribution in the vicinity of the polar front in winter. J. Meteorol. 5, 220–226.
Palmén, E., Newton, C.W., 1969. Atmospheric Circulation Systems. Their Structural and Physical Interpretation. Academic Press, New York, pp. 606.
Ran, M., Feng, Z., 2014. Variation in carbon isotopic composition over the past ca. 46,000 yr in the loess-paleosol sequence in central Kazakhstan and paleoclimatic significance. Org. Geochem. 73, 47–55.
Rao, Z.G., Chen, F.H., Zhang, X., Xu, Y.B., Xue, Q., Zhang, P.Y., 2012. Spatial and temporal variations of C_3/C_4 relative abundance in global terrestrial ecosystem since the Last Glacial and its possible driving mechanisms. Chin. Sci. Bull. 57, 4024–4035.
Rao, Z.G., Chen, F.H., Cheng, H., Liu, W.G., Wang, G.A., Lai, Z.P., Bloemendal, J., 2013a. High resolution summer precipitation variations in the western Chinese Loess Plateau during the last glacial. Sci. Rep. 3, 2785. https://doi.org/10.1038/srep02785.
Rao, Z.G., Xu, Y.B., Xia, D.S., Xie, L.H., Chen, F., 2013b. Variation and paleoclimatic significance of organic carbon isotopes of Ili loess in arid Central Asia. Org. Geochem. 63, 56–63.
Rao, Z.G., Guo, W.K., Cao, J.T., Shi, F.X., Jiang, H., Li, C.Z., 2017. Relationship between the stable carbon isotopic composition of modern plants and surface soils and climate: a global review. Earth Sci. Rev. 165, 110–119.
Rhodes, T.E., Gasse, F., Lin, R., Fontes, J.C., Wei, K., Bertrand, P., Gibert, E., Melieres, F., Tucholka, P., Wang, Z.X., Cheng, Z.Y., 1996. A Late Pleistocene-Holocene lacustrine record from Lake Manas, Zunggar (northern Xinjiang, western China). Palaeogeogr. Palaeoclimatol. Palaeoecol. 120, 105–121.
Seddon, A.W., Macias-Fauria, M., Long, P.R., Benz, D., Willis, K.J., 2016. Sensitivity of global terrestrial ecosystems to climate variability. Nature 531, 229–232.
Shi, Y.F., Shen, Y.P., Kang, E.S., Li, D.L., Ding, Y.J., Zhang, G.W., Hu, R.J., 2007. Recent and future climate change in northwest China. Clim. Chang. 80, 379–393.
Song, Y.G., Shi, Z.T., 2010. Distribution and compositions of loess sediments in Yili Basin, Central Asia. Sci. Geogr. Sin. 30, 267–272 (in Chinese with English abstract).
Song, Y.G., Shi, Z.T., Fang, X.M., Nie, J.S., Naoto, I., Qiang, X.K., Wang, X.L., 2010. Loess magnetic properties in the Ili Basin and their correlation with the Chinese Loess Plateau. Sci. China Earth Sci. 40, 61–72.
Soucek, S., 2000. A History of Inner Asia. Cambridge University Press, Cambridge.
Wang, W., Feng, Z.D., 2013. Holocene moisture evolution across the Mongolian Plateau and its surrounding areas: a synthesis of climatic records. Earth Sci. Rev. 122, 38–57.
Wang, G.A., Han, J.M., Liu, T.S., 2003. The carbon isotope composition of C_3 herbaceous plants in loess area of northern China. Sci. China Earth Sci. 46, 1069–1076.
Wang, G.A., Feng, X., Han, J.M., Zhou, L.P., Tan, W., Su, F., 2008. Paleovegetation reconstruction using $\delta^{13}C$ of soil organic matter. Biogeosciences 5, 1325–1337.
Wang, G.A., Li, J.Z., Liu, X.Z., Li, X.Y., 2013a. Variations in carbon isotope ratios of plants across a temperature gradient along the 400 mm isoline of mean annual precipitation in north China and their relevance to paleovegetation reconstruction. Quat. Sci. Rev. 63, 83–90.
Wang, W., Feng, Z.D., Ran, M., Zhang, C.J., 2013b. Holocene climate and vegetation changes inferred from pollen records of Lake Aibi, northern Xinjiang, China: a potential contribution to understanding of Holocene climate pattern in East-central Asia. Quat. Int. 311, 54–62.
Winkler, M.G., Wang, P.K., 1993. The late Quaternary vegetation and climate of China. In: Wright, H.E. (Ed.), Global Climates Since the Last Glacial Maximum. University of Minnesota Press, Minneapolis, pp. 221–261.
Wu, X., Huang, W., Chen, F.H., 2014. Construction and application of monthly air temperature and precipitation gridded datasets with high resolution ($0.025^\circ \times 0.025^\circ$) over China during 1951–2012. J. Lanzhou Univ. (Nat. Sci.) 50, 1–8 (In Chinese with English abstract).
Xia, D.S., Jia, J., Li, G.Q., Zhao, S., Wei, H.T., Chen, F.H., 2014. Out-of-phase evolution between summer and winter East Asian monsoons during the Holocene as recorded by Chinese loess deposits. Quat. Res. 81, 500–507.
Yang, S.L., Ding, Z.L., 2006. Winter-spring precipitation as the principal control on predominance of C_3 plants in Central Asia over the past 1.77 Myr: evidence from $\delta^{13}C$ of loess organic matter in Tajikistan. Palaeogeogr. Palaeoclimatol. Palaeoecol. 235, 330–339.
Yang, S.L., Forman, L.S., Song, Y.G., Pierson, J., Mazzocco, J., Li, X.X., Shi, Z.T., Fang, X.M., 2014. Evaluating OSL-SAR protocols for dating quartz grains from the loess in Ili Basin, Central Asia. Quat. Geochronol. 20, 78–88.
Ye, W., Sang, C.Q., Zhao, Y.X., 2003. Spatial-temporal distribution of loess and source of dust in Xinjiang. J. Desert Res. 23, 514–520 (in Chinese with English abstract).
Zhang, H.W., 2010. Variation in Organic Carbon Isotope Composition Values of Plant and Surface Soil along an Altitude Gradient in the Tienshan Mountains. (Doctorate dissertation).
Zhang, X.J., Jin, L.Y., 2016. Association of the Northern Hemisphere circumglobal teleconnection with the Asian summer monsoon during the Holocene in a transient simulation. The Holocene 26, 290–301.
Zhang, C.J., Chen, F.H., Jin, M., 2003a. Study on modern plant C_3 in western China and its significance. Chin. J. Geochem. 22, 97–106.
Zhang, Z.H., Zhao, M.X., Lu, H.Y., Faiia, A.M., 2003b. Lower temperature as the main cause of C_4 plant declines during the glacial periods on the Chinese Loess Plateau. Earth Planet. Sci. Lett. 214, 467–481.
Zhang, X.J., Jin, L.Y., Chen, J., Chen, F.H., Park, W., Schneider, B., Latif, M., 2017. Detecting the relationship between moisture changes in arid central Asia and East Asia during the Holocene by model-proxy comparison. Quat. Sci. Rev. 175, 36–50.
Zheng, S.X., Shangguan, Z.P., 2007. Spatial patterns of foliar stable carbon isotope compositions of C_3 plant species in the Loess Plateau of China. Ecol. Res. 22, 342–353.
Zhou, L.P., Oldfield, F., Wintle, A.G., Robinson, S.G., Wang, J.T., 1990. Partly pedogenic origin of magnetic variations in Chinese loess. Nature 346, 737–739.